Proposed Improvements in Response to Referee #1 Comments

Summary of Manuscript Revisions

To enhance physical robustness and statistical validation, the manuscript has been restructured by applying elements from Information Theory and Wavelet Transform Analysis (based on Mares et al., 2022). This framework allows for the significant separation and quantification of astronomical and radiative variables. Furthermore, discussions have been integrated directly into the results section to improve technical coherence and clarity.

The results obtained through this methodology—utilizing astronomical variables ($LP_0 = D\_au \times \sin(\delta)$), the Bivariate ENSO Timeseries (BEST), and CERES satellite data—provide robust validation for the proposed Relative Geoenergetic Equilibrium (RGE) Hypothesis.

Furthermore, the analysis reveals that both radiation (X_1) and astronomical variables (ΔLP) exhibit pure (*PWC*) and synergetic (*MWC*) significance in their coupling with the BEST index. Notably, during the 2023–2025 and 2005–2020 periods, clear synergies are observed in the 8–12-month band (centered at 10 months) and the 2–4-year interannual band (specifically between 2005–2010), alongside a high-frequency radiative response (1-month band) identified between 2000 and 2015.

These results are consistent across both hemispheres, with particularly strong signals at latitudes N +45.5° and S −45.5°, reinforcing the global validity of the proposed forcing mechanism. This modulation helps explain recent climate extremes, where the disruption of energetic equilibrium has altered global pressure center dynamics (GPA/LPA). The resulting destabilization produces anomalous precipitation and temperature regimes, including extreme snowfall in the Northern Hemisphere and prolonged droughts and wildfires in the Southern Hemisphere, consistent with the empirical satellite evidence presented. Likewise, the IRGON_Z index originally proposed in the preprint remains highly consistent with the Information Theory and Wavelet Transform Analysis methodology, contributing to the characterization of frequencies and amplitudes across each identified period.

The following points summarize the final structure of the manuscript contents. At the end of this document, the results related to the suggestions by Referee #1 are expanded upon. These additions have strengthened previous findings related to the primary hypothesis (*RGE*) and its implications. These updates not only reinforce the hypothesis but also support the title of the manuscript: *"Astroclimatic forcing of global climate dynamics and recent extremes: an integrated method and empirical satellite evidence of geo-orbital oscillation modulating ENSO."* Consequently, a new organizational structure has been proposed to provide the clarity and significance these findings merit.

2. Materials and Methods

2.1. Net Shortwave Radiation Dataset and Geophysical Proxies (Status: Preprint). The original Merra-ONI databases are maintained as the empirical foundation for net radiation analysis. This provides the historical context for shortwave radiation anomalies and their initial correlation with oceanic indices.

2.2. Satellite Imagery and Sunglint Observations (Status: Preprint). Visual evidence of solar–terrestrial geometry and specular reflection obtained through satellite sensors is utilized. This observational data serves as a qualitative proxy for the angular relationship between the Earth's surface and the solar vector.

2.3. Information Theory and Wavelet Transform Analysis (Status New: PWC–MWC Framework; after Mares et al.) The original cross-correlation analysis has been replaced by a more robust framework involving Multiple Wavelet Coherence (*MWC*) and Partial Wavelet Coherence (*PWC*). This approach isolates pure astronomical signals (ΔLP) from radiative variance (X_1) and quantifies non-linear synergies (S–R). Statistical validation is implemented using AR(1) red-noise models and Monte Carlo simulations, ensuring the results are robust against the serial autocorrelation inherent in the BEST index.

2.4. Spatial Radiative Gradients and Latitudinal Displacement (Status: Preprint + New). The interhemispheric radiative balance is quantified using CERES EBAF satellite data and the Lambert equation at monthly resolution. This section establishes the physical basis of the study, identifying the radiative gradient as the dynamic driver of the system. By analyzing flux at the centers of the Ferrel cells (±45.5°).

2.5. Index of Geo-Orbital Oscillation (IRGON) (Status: Preprint). The definition of the IRGON index is maintained as the primary descriptor of the fundamental geometric oscillation governing the astroclimatic coupling. The index represents the periodic variability in the Earth–Sun position vector, providing a benchmark for the frequency analysis performed in the wavelet domain.

3. Results and Discussion

3.1. Radiative and Geometric Evidence for Astroclimatic Modulation (Status: Preprint). This section provides a descriptive analysis of radiative variability across different ENSO phases, establishing the baseline for observed anomalies in the shortwave spectrum.

3.1.1. Net Downward Shortwave Radiation Variability During ENSO Phases (Status: Preprint). Detailed analysis of how net radiation fluctuates in response to tropical Pacific sea surface temperatures, identifying the characteristic "fingerprints" of radiative forcing during El Niño and La Niña events.

3.1.2. Spatial Radiative Gradients and Latitudinal Displacement (Status: Preprint + New Tables). The physical formulation for Top of the Atmosphere (TOA) incoming shortwave forcing utilizes the Lambert Law adapted to terrestrial spherical geometry and high-precision NASA ephemerides. The instantaneous solar irradiance (Q) at a specific latitude (φ) is defined by the solar elevation angle (α) as: $Q = (S_0 / r^2) \cdot \sin(\alpha)$. To reconcile the 10^{-4} paradox with observed MERRA-2 and CERES EBAF anomalies, a Temporal Amplification Factor ($\Gamma \approx 12$) is applied to mid-latitudes (±45.5°) as a comparative approximation. This factor integrates the diurnal cycle, the monthly persistence of the solar declination (δ) shift, and latitudinal sensitivity, where millesimal changes in δ alter both intensity and photoperiod duration. Consequently, the latitudinal shift of the radiative maximum breaks equatorial thermal symmetry, acting as the initial dynamic trigger for global energy redistribution. This geometric modulation provides the physical basis for the phase transitions identified through both the IRGON model and the Information Theory and Wavelet Transform analysis (Mares et al., 2022), linking orbital kinematics with climate responses. This specific formulation is presented as a complementary theoretical framework; all primary variables utilized in the subsequent statistical analyses (PWC, NLR, and IRGON) consist of raw observational and ephemeris data as specified in their respective sections.

3.1.3. Satellite Imagery and Sunglint Observations (Status: Preprint). Geometric validation of observation windows through specular reflection (sunglint). These observations confirm the precise solar–terrestrial alignment required for the proposed modulation mechanism.

3.2. Multiscale Oscillatory Coherence and Principal Bands (Status New: After Mares et al.). Following the Referee#1 recommendation, the original Cross-Correlation Function (CCF) has been replaced by an Information Theory and Wavelet Transform framework (Mares et al., 2022). By isolating the pure mutual information (MI) between the geo-orbital oscillation (ΔLP) and the BEST index, we successfully removed redundant solar variance. Statistical significance in the 2–4-year and 10-month bands persists under rigorous AR(1) red-noise modeling and Monte Carlo testing ($p < 0.05$).

3.3. IRGON Model: Geo-Orbital Oscillation Analysis (Status: Preprint + New Figures). Evaluation of the diagnostic capability of the IRGON index to anticipate shifts in global climate dynamics. New figures demonstrate the high degree of phase-locking between the index's geometric oscillations and major shifts in the BEST index.

3.4. The Orbital Differential between Equinoxes (*ΔLP*) (Status: Preprint + New Comments). To address the distance paradox (10^{-4}), we apply the ΔLP component (Lateral Projection of the Earth–Sun position vector). This represents the Earth's spatial displacement relative to the solar equatorial plane at the specific moment of the September equinox. The component is defined as: $LP_0 = D\_au \times \sin(\delta) \times 149{,}597{,}870.7$ Where D_au is the instantaneous Earth–Sun distance in astronomical units, and δ is the solar declination. The resulting ΔLP effectively translates astronomical scales into terrestrial-scale displacements (km).

3.5. Relative Geoenergetic Equilibrium (RGE) Hypothesis (Status: Preprint). This section integrates the findings into a physically plausible mechanism. The RGE hypothesis explains how interannual variations in heliocentric distance and declination—particularly during the September equinox window—are amplified by the latitudinal redistribution of energy. This forces the climate system to adjust its momentum and seek a new equilibrium. This process occurs during periods of significant coupling between astronomical position (ΔLP) and radiative energy (X_1) over open ocean regions, as evidenced by the high synergy observed in the ONI and BEST indices.

Detailed Results and Supplementary Material

Supplementary tables, multiscale coherence plots, and a supporting bibliography are included to sustain the restructuring of the manuscript. The following sections detail the methodology, results, and discussions of the primary points labeled as Status: New, which significantly strengthen the physical and statistical foundation of the study. The figures and charts are numbered chronologically within this document for clarity, but will be integrated into their respective sections in the final version of the manuscript**.**

Methods

3.2. Multiscale Oscillatory Coherence and Principal Bands (Status: New after Mares et al.)

To address the non-linear and non-stationary nature of the climate system, this study adopts the framework proposed by Mares et al. (2022), which integrates Information Theory with advanced Wavelet Transform techniques to isolate the influence of astronomical forcing from radiative variables. Within this methodology, the coupling between the predictors (X_1: radiation; X_2: astronomical variable) and the predictand (Y: BEST index) is evaluated using the Non-linear Correlation Coefficient (NLR), derived from Mutual Information (MI):

$$\mathrm{NLR} = \sqrt{(1 - \exp(-2MI))} \qquad (1)$$

MI indicates the amount of information shared between two time series, allowing for the detection of dependencies regardless of the statistical distribution of the variables. The dataset comprises a continuous series of 310 months (2000–2025), with seasonal analysis performed on subsets of 78 values per station (e.g., SON). For the Pearson correlation coefficient, confidence levels were determined using standard tables for series of this length. Following the framework of Mares et al., the 95% confidence levels for the NLR and S–R metrics were established according to the methodologies of Steuer et al. and Theiler et al., ensuring the statistical significance of the non-linear dependencies and synergistic interactions identified.

To further quantify the relative contribution of each predictor, a Synergy–Redundancy (S–R) analysis is implemented following Timme et al. (2014):

$$\text{S–R} = \text{Synergy}\ (Y; X_1, X_2) - \text{Redundancy}\ (Y; X_1, X_2) \tag{2}$$

$$\text{S–R} = MI(X_1, X_2; Y) - MI(X_1; Y) - MI(X_2; Y) \tag{3}$$

A positive S–R value indicates that the combined influence of radiation and orbital kinematics exceeds the sum of their independent contributions, identifying a phase-locked synergy between the variables. Conversely, a negative value implies that the redundant contribution is greater in magnitude than the synergetic contribution. Furthermore, we estimate the Total Correlation (TC) between all variables as:

$$\text{TC} = MI\ (X_1; X_2) + MI\ (X_1, X_2; Y) \tag{4}$$

Where X_1 represents the CERES incoming solar flux (EBAF Ed4.2) at ±45.5° (Ferrel cell mass centers). By selecting this variable as the primary signal, stochastic variability associated with atmospheric processes and oceanic feedbacks is substantially reduced. X_2 corresponds to the astronomical variable defined as the interannual orbital displacement ΔLP ($\Delta LP_n = LP_0(n) - LP_0(n-1)$), where $LP_0 = D\_au \times \sin(\delta)$. The predictand Y represents the Bivariate ENSO Timeseries (BEST) index (Smith and Sardeshmukh, 2000).

To resolve these interactions in the time–frequency domain, the analysis employs Multiple Wavelet Coherence (*MWC*) to identify the total coherence between both predictors and the climate index. Complementarily, Partial Wavelet Coherence (*PWC*) is applied to isolate the pure astronomical component. As demonstrated by Hu and Si (2021), *PWC* allows for the detection of scale-dependent coherence and lag relationships between two variables while removing the influence of the remaining variables, effectively separating radiative variability from the orbital signal.

The statistical robustness of the results is ensured through several validation procedures. First, AR(1) red-noise modeling is used to account for the serial autocorrelation inherent in the BEST index. Second, Monte Carlo simulations are performed to establish the 95% confidence level, represented by black contour lines in the wavelet coherence plots. Finally, cross-lag optimization is conducted by testing lags months, based on the highest TC and S–R values. This procedure identifies the operational temporal windows in which the coupled radiation–astronomical system exerts its strongest influence on global energy redistribution.

Results and Discussion

3.2. Multiscale Oscillatory Coherence and Principal Frequency Bands

3.2.1. Comparison of Linear and Non-linear Correlations, Synergy–Redundancy (S–R) and Total Correlation (TC)

Following the methodology of Mares et al. (2022), we first compared the linear (Pearson) and non-linear (NLR) relationships between the astro-radiative predictors and the climate response. The results demonstrate that NLR values are consistently higher than the absolute linear correlation |R| across all analyzed lags (0–10 months), as illustrated in Figure 1. This prevalence of non-linear dependencies aligns with the findings of Le Mouël et al. (2019), who identified robust solar and astronomical signatures across multiple climate indices that are often obscured or attenuated when utilizing strictly linear methods.

For the September equinox (SON), the NLR remains substantially above the 95% confidence level (NLR > 0.25), peaking at lags of 5 and 6 months with values of approximately 0.51 and 0.50, respectively (see Table 1). In contrast, the linear correlation |R| remains consistently near or below the significance threshold (~0.12), with a maximum of only 0.13 at lag 6.

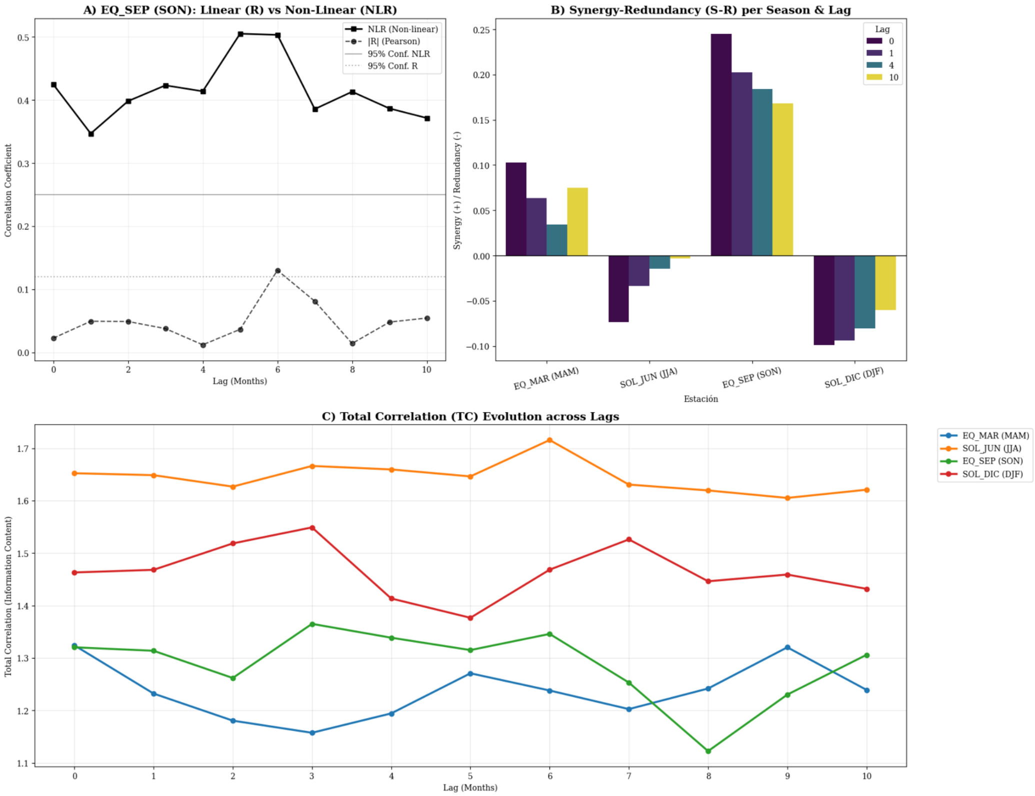

Figure 1 Linear vs. Non-linear Correlation Evolution. Comparison between Pearson |R| and NLR for the SON window across lags 0–10. The shaded area/dashed line represents the 95% confidence interval established via Monte Carlo simulations.

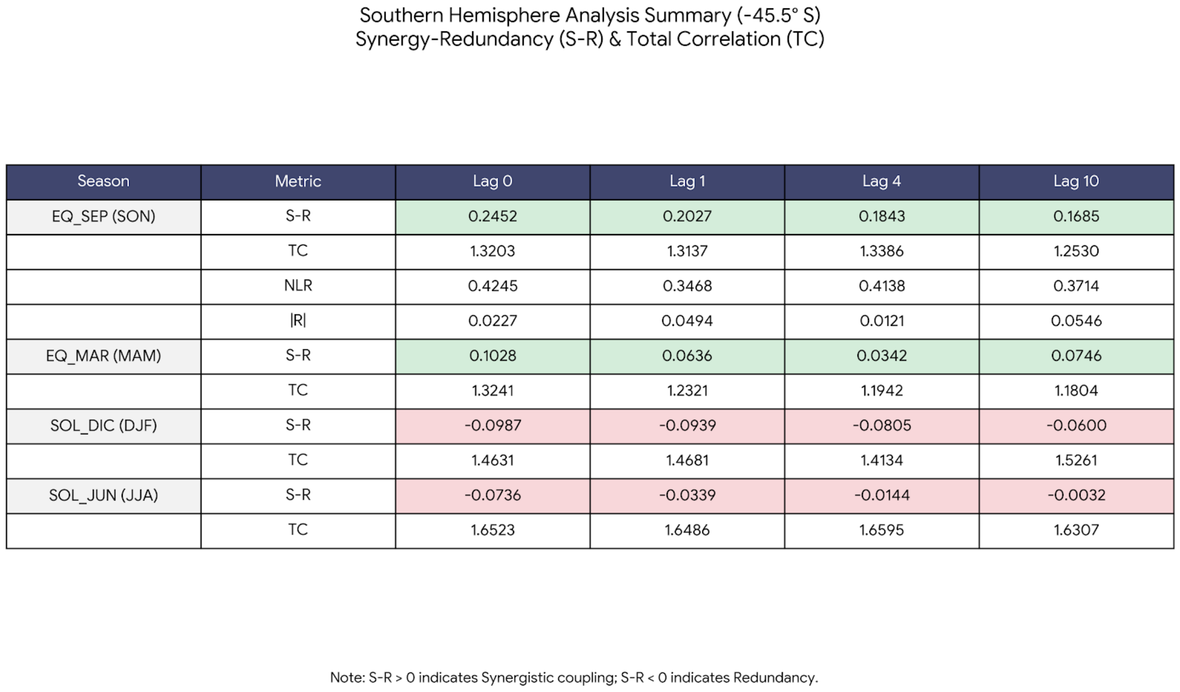

Southern Hemisphere Analysis Summary (-45.5° S)
Synergy-Redundancy (S-R) & Total Correlation (TC)

Season	Metric	Lag 0	Lag 1	Lag 4	Lag 10
EQ_SEP (SON)	S-R	0.2452	0.2027	0.1843	0.1685
	TC	1.3203	1.3137	1.3386	1.2530
	NLR	0.4245	0.3468	0.4138	0.3714
	|R|	0.0227	0.0494	0.0121	0.0546
EQ_MAR (MAM)	S-R	0.1028	0.0636	0.0342	0.0746
	TC	1.3241	1.2321	1.1942	1.1804
SOL_DIC (DJF)	S-R	-0.0987	-0.0939	-0.0805	-0.0600
	TC	1.4631	1.4681	1.4134	1.5261
SOL_JUN (JJA)	S-R	-0.0736	-0.0339	-0.0144	-0.0032
	TC	1.6523	1.6486	1.6595	1.6307

Note: S-R > 0 indicates Synergistic coupling; S-R < 0 indicates Redundancy.

Table 1 Synergy–Redundancy (S–R) and Total Correlation (TC) Metrics. Seasonal values for the equinoctial (SON) and solstitial (JJA, DJF) windows at key lags. Positive S–R denotes synergistic information transfer, while negative values indicate redundancy.

This confirms that the coupling between orbital-geometric perturbations (ΔLP) and the BEST index (Y) is predominantly non-linear and deterministic.

The simultaneous influence of the two predictors (X_1: Radiation and X_2: ΔLP) was evaluated by calculating the difference between synergy and redundancy (S–R) and the Total Correlation (TC) (Table 1):

- **Equinoctial Synergy:** A distinctive feature is observed during the September equinox (EQ_SEP), where S–R reaches its maximum positive value of 0.2452 at lag 0 and remains strongly synergistic at lag 1 (0.2027), as detailed in Table 1. This positive value confirms that the combined action of radiative flux (X_1) and orbital displacement (ΔLP) provides significantly more information about climate variability than each predictor independently, identifying a phase-locked coupling operational window. Based on the maximum TC and S–R peaks, lags of 0, 1, 4, and 10 months were selected for in-depth analysis. Lags 0 and 1 capture the immediate thermodynamic response and the peak of synergistic coupling during the SON window, while lags 4 and 10 months represent the seasonal transition and the nearly annual memory of the system, respectively, aligning with the 10-month oscillatory band identified in the wavelet analysis.

- **Solstitial Redundancy:** Conversely, the solstitial seasons exhibit predominantly negative S–R values. During the June solstice (JJA), redundancy reaches −0.0736 at lag 0, while the December solstice (DJF) shows even greater redundancy, reaching −0.0987. This implies that during solstices, the astronomical signal becomes redundant with the seasonal radiative cycle, providing overlapping rather than synergistic information.

- **Total Dependency:** Maximum TC values exceed 1.70 during the June solstice (JJA) at a 6-month lag. While this indicates a strong total dependency among variables, the negative S–R suggests the system is driven by radiative redundancy during this period, whereas the SON window provides the most efficient information transfer.

These findings validate that the high-coherence patterns identified in the wavelet analysis are not stochastic noise. Instead, they represent a synergistic astroclimatic modulation that peaks during the Southern Hemisphere spring, acting as the primary driver for the redistribution of global geoenergetic equilibrium.

3.2.2 Multi-Scale Wavelet Transform Analysis: MWC and PWC

To detail the time–frequency distribution of these relationships, we applied Multiple Wavelet Coherence (MWC) and Partial Wavelet Coherence (PWC) for the Southern Hemisphere validation at −45.5° S. This multiscale approach isolates the specific contribution of astronomical forcing (ΔLP) across different operational windows.

- **MWC (Synergetic Coupling):** Significant coherent bands are identified in the 2–4 year interannual range and the 8–12 month band, centered at 10 months. The synergy is most evident during the 2005–2010 and 2023–2025 periods, where the combined predictors reach statistical significance, surviving the AR(1) red-noise test (indicated by black contours).

- **PWC Astro (The Pure Signal):** When excluding radiative variance (X_1), a persistent coherent structure remains in the 2–4 year frequency band, particularly evident at lags 4 and 10 months. This "pure" astronomical signal identifies an independent orbital modulation of the global BEST index (Y) that is not merely a reflection of solar flux.

- **Lag Dynamics and Phase-Locking:** The analysis of optimal lags (0, 1, 4, and 10 months) reveals a phase-locked response. At lag 0 and 1, the system shows immediate high-frequency sensitivity. By lag 10, the coherent region in the PWC Astro field becomes broader and more intense, identifying a delayed operational window for the dissipation of the orbital kinematic shock within the Ferrel cell domain.

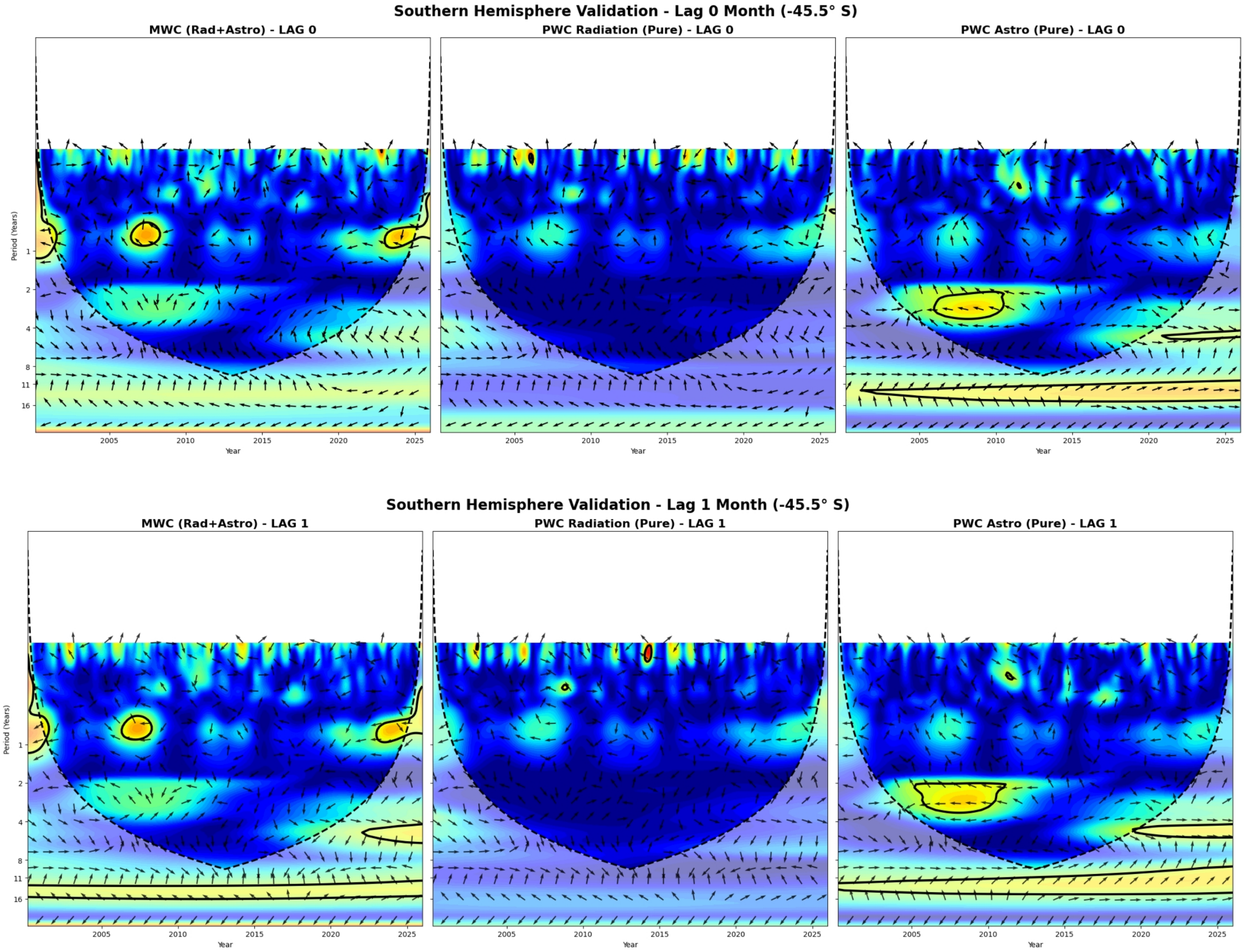

Figure 2 High-Frequency Synergy (Lags 0 & 1) during the SON Season at –45.5° S. MWC and PWC plots showing the immediate coupling during the 2023–2025 period. The black contours denote the 95% confidence level against red noise, validating the synergetic interaction during the September equinox window.

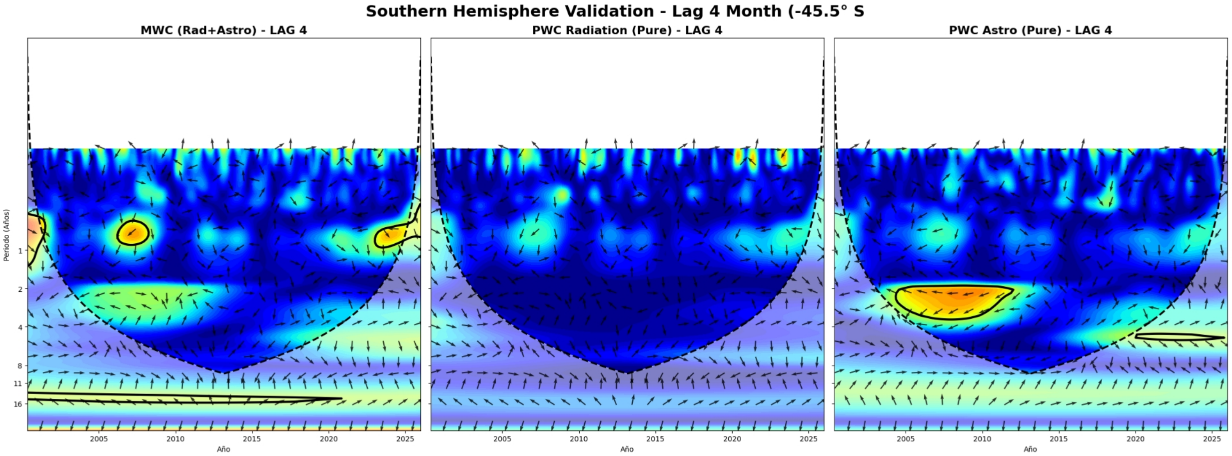

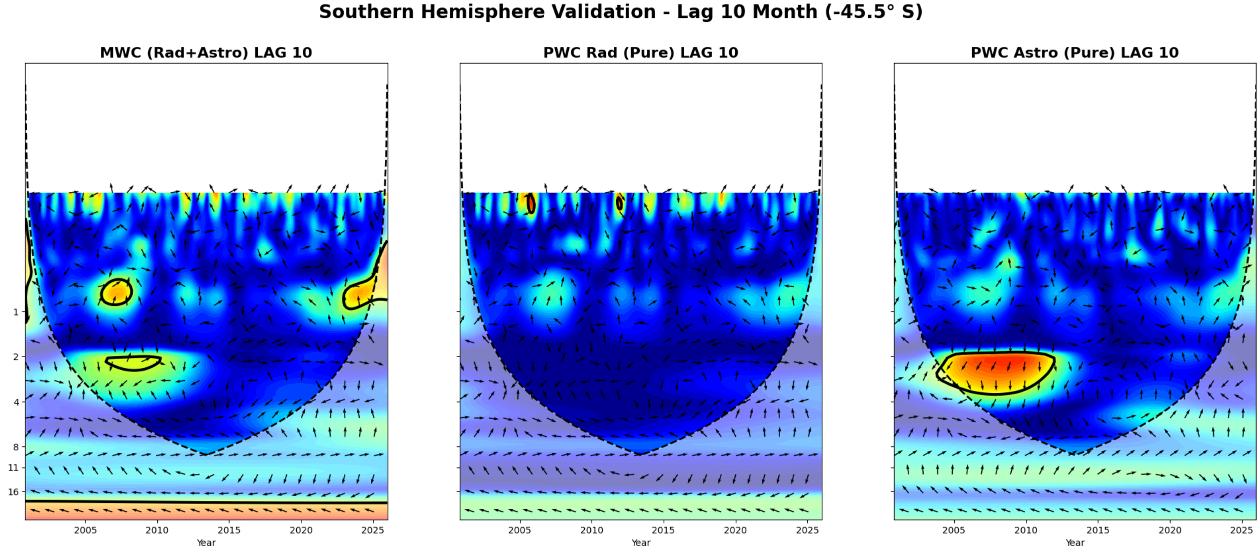

Figure 3 Interannual and 10-month Modulation (Lags 4 & 10) during the SON Season at –45.5° S. At lag 10, the PWC Astro signal (right panel) demonstrates its maximum intensity and breadth in the 2–4 year band, confirming the "pure" astronomical influence of *ΔLP* on the BEST index (*Y*) during the spring quarter.

These findings confirm that the recent 2023–2025 anomalies are not stochastic noise but are part of a deterministic phase-locked synergy between radiative energy and orbital kinematics. This modulation, characterized by the 10-month and 2–4 year bands, provides the statistical validation for the Relative Geoenergetic Equilibrium (RGE) hypothesis, suggesting a high-magnitude climate adjustment for the 2026 period.

The application of the MWC–PWC framework to the Northern Hemisphere at +45.5° N confirms the global scale of the identified astro-radiative modulation. The results exhibit high consistency with the Southern Hemisphere patterns, identifying significant coherent structures in the 8–12 month and 2–4 year bands. This interhemispheric symmetry reinforces the hypothesis that the geo-orbital oscillation (ΔLP) acts as a primary driver of the global energy redistribution, with the most intense coupling appearing in phase-locked windows during the 2005–2010 and 2023–2025 periods. The robustness of these results across both hemispheres, surviving the AR(1) red-noise threshold, demonstrates that the identified frequencies are a deterministic feature of the coupled climate system rather than local stochastic variability.

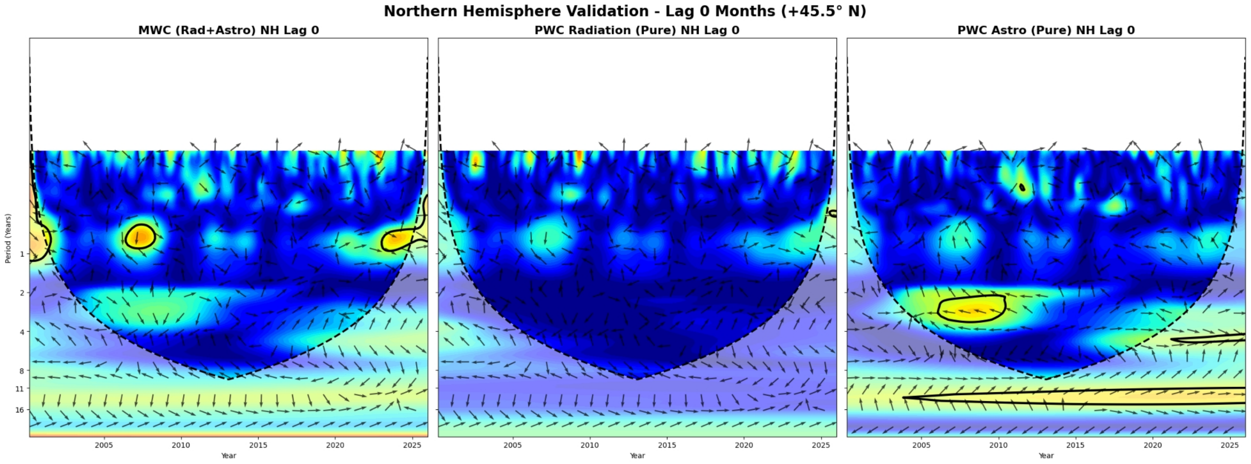

Northern Hemisphere Validation - Lag 0 Months (+45.5° N)

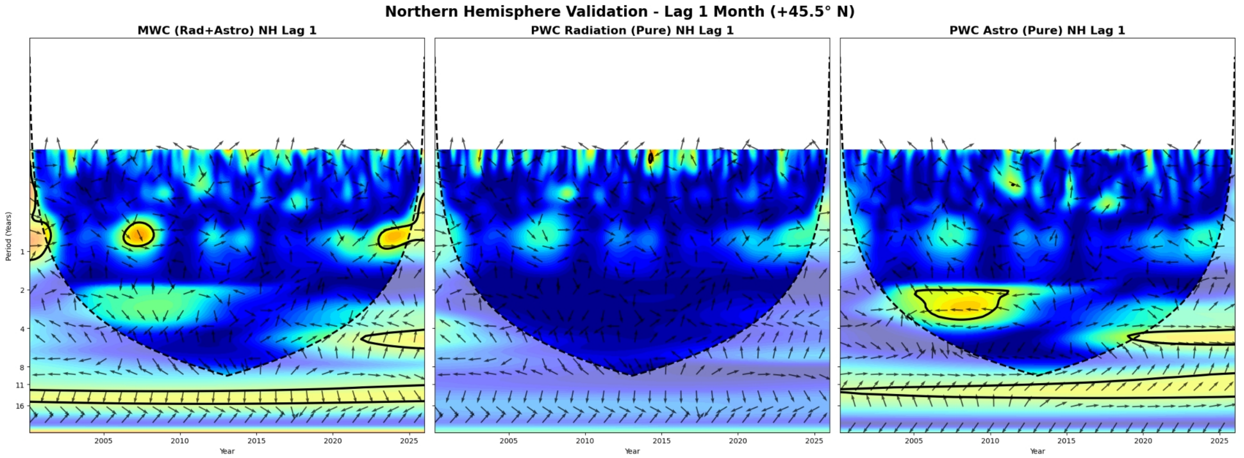

Northern Hemisphere Validation - Lag 1 Month (+45.5° N)

Figure 4 Northern Hemisphere Synergy and Immediate Response (Lags 0 & 1) at +45.5° N**.** MWC and PWC analysis at +45.5° N showing significant phase-locked synergy during the 2023–2025 period. The black contours indicate the 95% confidence level, identifying the radiative and astronomical components' simultaneous influence on the climate index.

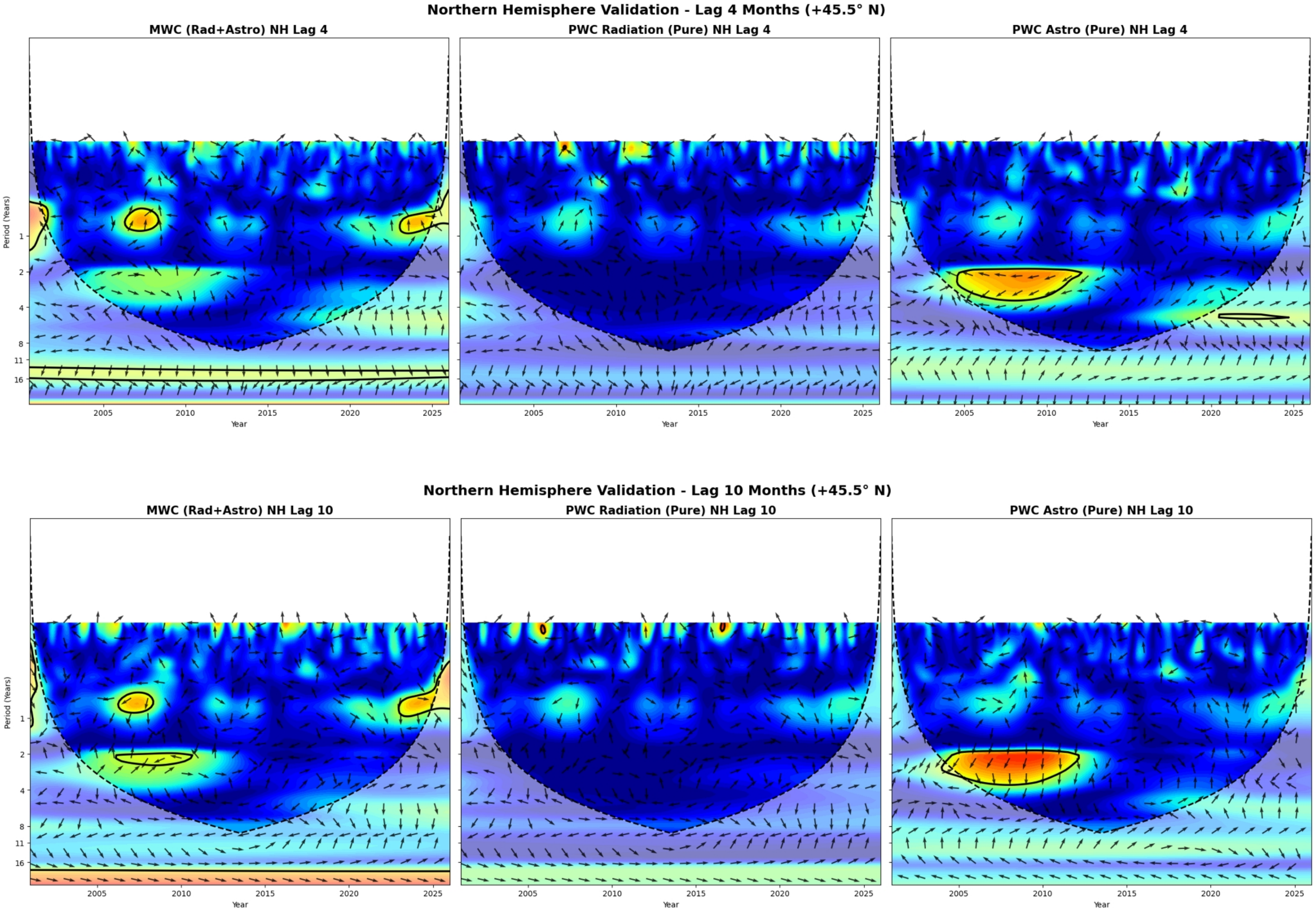

Figure 5 Interannual Orbital Modulation in the Northern Hemisphere (Lags 4 & 10) at +45.5° N**.** Consistent with the Southern Hemisphere results, the PWC Astro signal at lag 10 months reveals a broad and persistent significance in the 2–4 year band. This confirms the existence of a "pure" astronomical signal influencing Northern Hemisphere climate dynamics independently of direct radiative variance.

3.3. IRGON Model: Assessing Astroclimatic Oscillatory Periods through Information Theory (Status: Preprint + Added Figure and Commentary)

The original Wavelet analysis has been replaced with a robust Information Theory framework, following the methodologies established by Mares et al. (2022). This transition is necessitated by the requirement to isolate independent astronomical forcing from complex radiative responses—a task where conventional spectral methods frequently fail to distinguish between coupled variables. This updated approach quantifies the non-linear coupling and the deterministic Information Flow from geo-orbital parameters to the ocean-atmosphere system, specifically the ONI and BEST indices.

Furthermore, this methodology operates across two levels of information where periodic coherences are observed: the Information Theory analysis utilizes Top of Atmosphere (TOA) or Incoming Flux data at mid-latitudes, while the IRGON model utilizes radiation data specifically at the Open Waters level within the ONI zone. In both cases, the phases and periods remain highly consistent, validating the physical drivers across different atmospheric layers (see Figure 6).

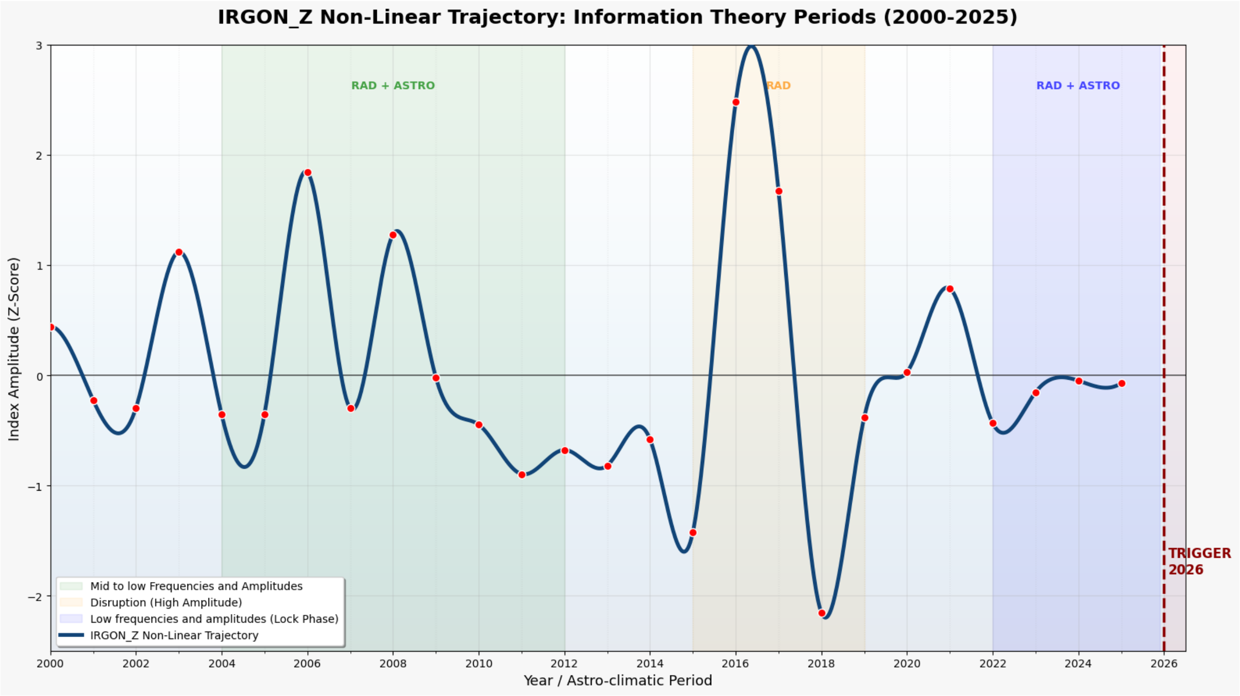

Figure 6. IRGON_Z Non-Linear Oscillation Trajectory: Significance periods derived from Information Theory and Wavelet Transform Analysis.The plot illustrates index frequencies and amplitudes per period, identifying specific intervals of astroclimatic coupling where the orbital signal overrides stochastic noise.

Analyzing the non-linear behavior of the IRGON_Z index through this lens identifies specific patterns of coupling:

- **Identification of Frequency and Amplitude Patterns:** The information-based analysis deconstructs the historical record into distinct physical phases. This reveals clear periods of high informative disruption—such as the 2016 pulse where IRGON_Z reached 2.47—contrasted with phases of low amplitude or "tense stability," as observed in the current 2022–2025 coupling.

- **Validation of Non-Linear Causality:** Moving beyond simple linear correlations, Information Theory confirms that IRGON_Z accurately detects when the climate system receives an orbital information pulse strong enough to force a phase transition. The synergy between orbital distance and solar declination acts as the deterministic driver, establishing a clear cause-and-effect mechanism.

- **The 2024–2025 Lock Phase and the 2026 Trigger:** The analysis detects that during 2024 and 2025, the system entered a period of maximum information transfer and low entropy. This informative stability does not represent inactivity, but rather a significant coupling state period that serves as the precursor to the 2026 trigger.

Finally, a primary mechanism through which these astroclimatic oscillations influence global climate is the modulation of oceanic pressure centers, affecting both their location and magnitude. This is evidenced by analyzing spatial-temporal correlations between Top of the Atmosphere (TOA) incoming shortwave flux from MERRA-2 data and Sea Level Pressure (SLP). These correlations reveal significant shifts in core pressure centers during key periods: September–December 2018 (El Niño), 2022 (La Niña), and 2025 (Neutral-to-Niña transition). These spatial patterns do not contradict the non-linear nature of the system; rather, they represent the atmospheric bridge where deterministic astroclimatic forcing manifests as organized climate responses.

Physically, the 2025 lock or astroclimatic coupling represents a state of minimum entropy. This state is expressed as periods of intensified effects characterized by higher synergy and lower redundancy between astronomical and radiative variables. The high-resolution alignment between TOA flux and surface pressure centers indicates that the climate system has ceased to exhibit relevant stochastic fluctuations. This state of continuous coupling within a specific period—where the system is effectively "trapped" by its orbital geometry—facilitates the phase transition observed in early 2026.

As the accumulated geo-orbital energy is released into a new radiative equilibrium, the system undergoes the abrupt shift that characterizes the "Ice and Fire" events of early 2026. This transition is marked by displaced and concentrated pressure centers in critical climatic zones, as documented in the provided imagery. These changes affect multiple areas across mid-latitudes and equatorial regions, displacing the polar effect toward lower latitudes in the Northern Hemisphere (NH), while in the Southern Hemisphere (SH), it significantly reduces precipitation in areas such as the South American Pampas, the Patagonian Andes, and Australia.

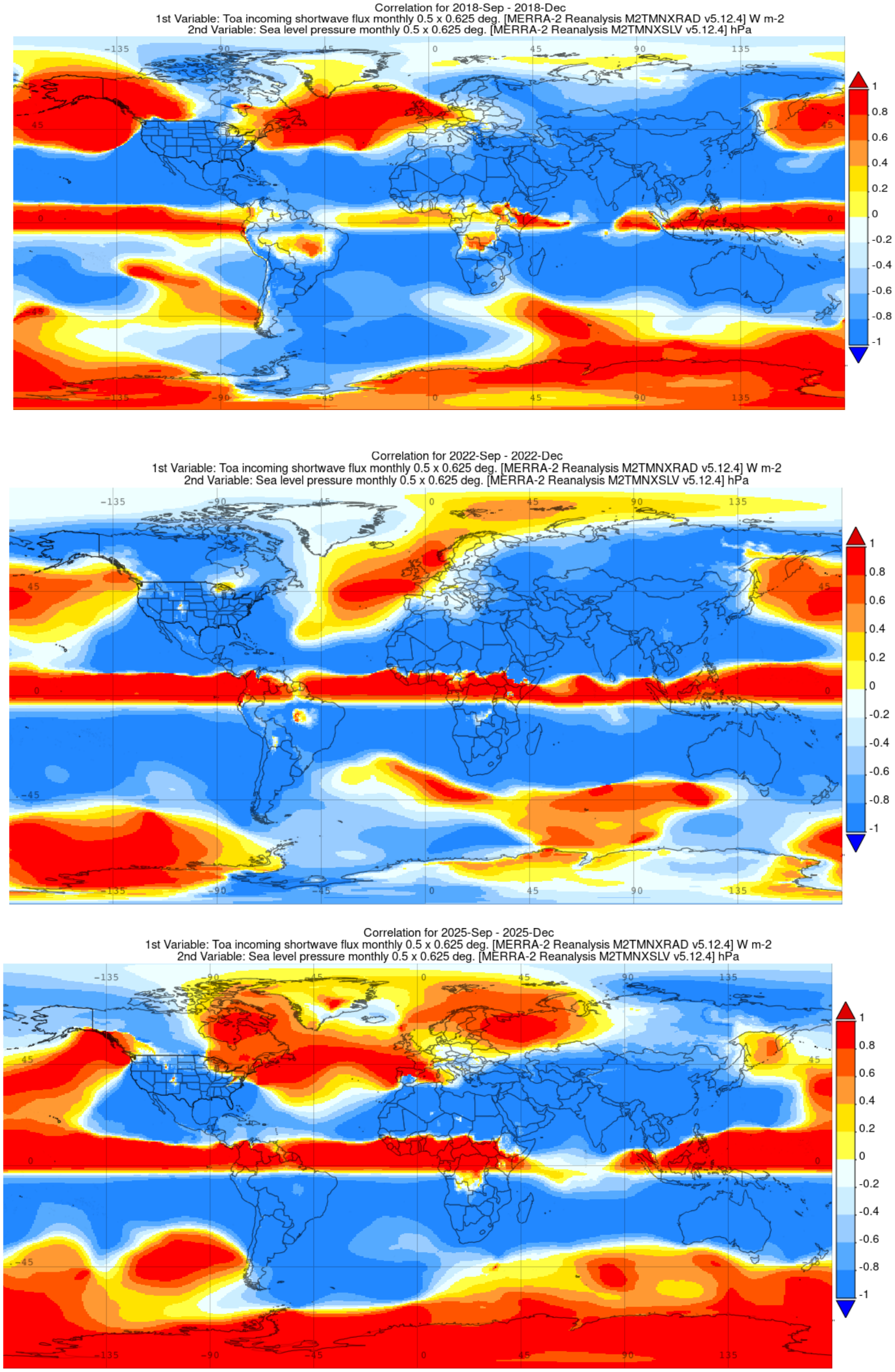

Correlation for 2018-Sep - 2018-Dec
1st Variable: Toa incoming shortwave flux monthly 0.5 x 0.625 deg. [MERRA-2 Reanalysis M2TMNXRAD v5.12.4] W m-2
2nd Variable: Sea level pressure monthly 0.5 x 0.625 deg. [MERRA-2 Reanalysis M2TMNXSLV v5.12.4] hPa

Correlation for 2022-Sep - 2022-Dec
1st Variable: Toa incoming shortwave flux monthly 0.5 x 0.625 deg. [MERRA-2 Reanalysis M2TMNXRAD v5.12.4] W m-2
2nd Variable: Sea level pressure monthly 0.5 x 0.625 deg. [MERRA-2 Reanalysis M2TMNXSLV v5.12.4] hPa

Correlation for 2025-Sep - 2025-Dec
1st Variable: Toa incoming shortwave flux monthly 0.5 x 0.625 deg. [MERRA-2 Reanalysis M2TMNXRAD v5.12.4] W m-2
2nd Variable: Sea level pressure monthly 0.5 x 0.625 deg. [MERRA-2 Reanalysis M2TMNXSLV v5.12.4] hPa

Figure 7 Comparison of atmospheric responses during key astroclimatic windows: (Top) September–December 2018; (Middle) September–December 2022; and (Bottom) September–December 2025. The shifting intensity and location of the core pressure centers demonstrate the atmospheric bridge through which the orbital-geometric coupling forces the 2026 phase transition.

3.4. The Orbital Differential between Equinoxes (ΔLP) (Status: NEW)

To address the apparent paradox regarding the small magnitude of astronomical variations (the 10^{-4} scale) and their disproportionate impact on climate, the analytical focus is redefined from gross energy changes to geometric precision. The LP_0 component (lateral projection of the Earth–Sun position vector) is defined as the Earth's spatial displacement relative to the solar equatorial plane at the exact moment of the September equinox (Day 0). This component represents the latitudinal projection of the Earth–Sun vector and is defined as:

$$LP_0 = D\_au \times \sin(\delta) \times 149{,}597{,}870.7 \qquad (5)$$

Where:

- ***D_au*** is the instantaneous Earth–Sun distance in astronomical units (AU).
- ***δ*** (Solar Declination) is the angle relative to the equatorial plane.

Interannual Kinematic Variation. The interannual displacement is defined as the change in Earth's lateral position relative to the solar equatorial plane between consecutive equinoxes:

$$\Delta LP_n = LP_0(n) - LP_0(n-1) \qquad (6)$$

Ephemerides from NASA Horizons and IMCCE show a marked increase in this displacement over the last two decades:

- Year 2000: $\Delta LP \approx 8{,}269$ km
- Year 2024: $\Delta LP \approx 353{,}509$ km
- Year 2025: $\Delta LP \approx 360{,}535$ km

Compared with the near-equatorial configuration around 2000, this represents a massive increase of approximately 4,000% in the lateral displacement component. These ΔLP values were utilized as the astronomical variable (X_2) in the Partial Wavelet Coherence (PWC) framework, combined with CERES satellite radiation data and the BEST index (Y), producing the statistically significant coherence signals discussed in Section 3.2.

Synchronization Mechanism

The proposed mechanism is not based on gross radiative forcing but on phase coupling between net shortwave radiation variability and orbital-geometric displacement. The massive spatial projection of the Earth–Sun vector (≈360,000 km, a distance comparable to the Earth–Moon separation) modifies the timing and latitudinal distribution of the solar zenith angle, altering radiative gradients over the oceans. This geometric modulation acts as a kinematic driver for energy redistribution within the climate system.

This coupling is a fundamental component of the Relative Geoenergetic Equilibrium (RGE) of the climate system, particularly affecting the Ferrel cell domain (±45.5° latitude) and modifying global pressure centers. These dynamical adjustments are consistent with observed anomalies in precipitation and temperature during recent extreme climate events (2023–2025), providing a deterministic link between orbital kinematics, radiative gradients, and large-scale atmospheric circulation variability.

New References

Hu, W.; Si, B.C. Multiple wavelet coherence for untangling scale-specific and localized multivariate relationships in geosciences. Hydrol. Earth Syst. Sci. 2016, 20, 3183–3191.

Le Mouël, J.-L., Lopes, F., and Courtillot, V. (2019). A solar signature in many climate indices. *Journal of Geophysical Research: Atmospheres*, 124(5), 2600–2619. https://doi.org/10.1029/2018JD028939

Mares, C., Dobrica, V., Mares, I., and Demetrescu, C. (2022). Solar Signature in Climate Indices. *Atmosphere*, 13(11), 1898. https://doi.org/10.3390/atmos13111898

Smith, C. A., and Sardeshmukh, P. D. (2000). The Effect of ENSO on the Intraseasonal Variance of Surface Temperature in Winter. *International Journal of Climatology*, 20(13), 1543–1557. https://doi.org/10.1002/1097-0088(20001115)20:13<1543::AID-JOC580>3.0.CO;2-4

Steuer, R., Kurths, J., Daub, C. O., Weise, J., and Selbig, J. (2002). The mutual information: Detecting and evaluating dependencies between variables. *Bioinformatics*, 18(Suppl_2), S231–S240. https://doi.org/10.1093/bioinformatics/18.suppl_2.S231

Theiler, J., Eubank, S., Longtin, A., Galdrikian, B., and Farmer, J. D. (1992). Testing for nonlinearity in time series: The method of surrogate data. *Physica D: Nonlinear Phenomena*, 58(1-4), 77–94. https://doi.org/10.1016/0167-2789(92)90102-S

Timme, N., Alford, W., Flecker, B., and Beggs, J. M. (2014). Synergy, redundancy, and multivariate information measures: An experimentalist's perspective. *Journal of Computational Neuroscience*, 36(2), 119–140. https://doi.org/10.1007/s10827-013-0458-4